

Characterization of a Superconducting nanowire single photon detector

Max Reicherd

Bachelorarbeit in Physik
angefertigt im Institut für Angewandte Physik

vorgelegt der
Mathematisch-Naturwissenschaftlichen Fakultät
der
Rheinischen Friedrich-Wilhelms-Universität
Bonn

Juli 2024

I hereby declare that this thesis was formulated by myself and that no sources or tools other than those cited were used.

Bonn,
Date
Signature

1. Reviewer: Prof. Dr. Sebastian Hofferberth
2. Reviewer: Prof. Dr. Daqing Wang

Acknowledgements

I would like to thank ...

You should probably use \chapter* for acknowledgements at the beginning of a thesis and \chapter for the end.

Contents

1	Introduction	1
2	Working principle of SNSPDs	2
3	Faint laser source for detector characterization	5
3.1	Characteristics of faint laser sources	5
3.2	Experimental setup	6
4	Characterization of a SNSPD by single Quantum	9
4.1	Dark Count Rate	9
4.2	Recovery time	11
4.3	Efficiency	15
4.4	Discussion	18
5	Conclusion and Outlook	19
A	Appendix	20
	Bibliography	21

CHAPTER 1

Introduction

CHAPTER 2

Working principle of SNSPDs

In its essence, the SNSPD consists of four parts, seen in fig. 2.1. A sapphire underground, a detection area made out of a superconducting nanowire in a serpentine winding and placed onto the sapphire underground, a gold contact to supply a bias current through the superconducting nanowire and a fiber coupled to the detection area.

The sapphire layer is used to efficiently dissipate the heat when the wire heats up.

Moreover, the set up is first cooled below the critical temperature of the superconductor ($2 - 3\text{K}$), and a bias current is applied to the superconductor that is lower than the critical current.

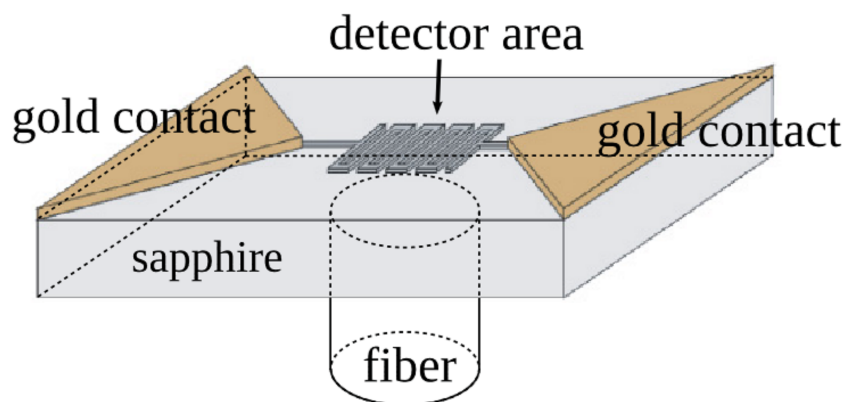


Figure 2.1: (a) Schematic structure of a superconducting nanowire single photon detector [1]

The detection process can be understood along the detection circle in fig. 2.2.

Single photons hitting a superconducting nanowire (ii) and break up individual Cooper pairs. This leads to a local reduction of the critical current below the bias current and in turn to a localised area where the superconductivity is interrupted, this local area forms the so-called "hotspot" (iii). This hotspot forms a resistance area because the bias current exceeds the critical current. In response, the current flows around this hotspot (iv), whereby the local current density in the side areas next to the hotspot again exceeds the critical current, due to a higher current density. This excess also causes a

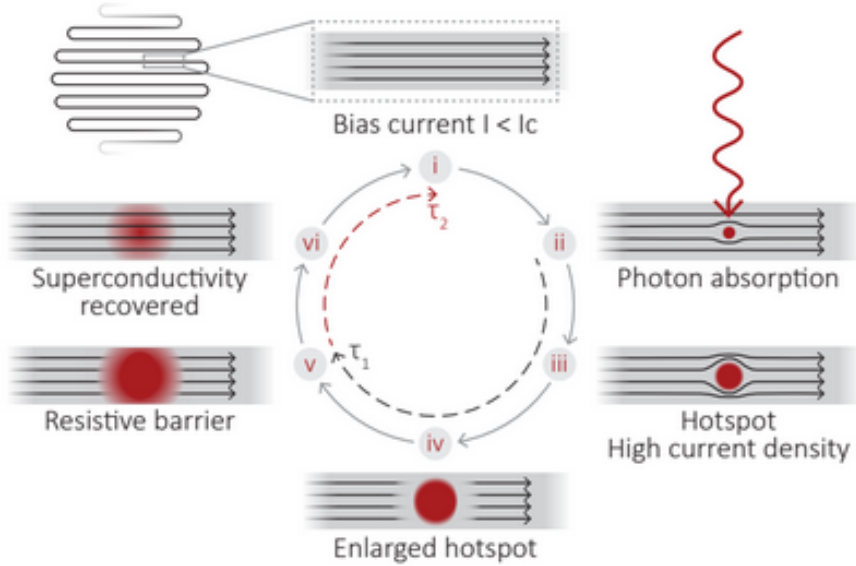


Figure 2.2: Schematic detection cycle of a superconducting nanowire single photon detector [2]

resistance in the side channels due to the critical temperature being exceeded (v). Ultimately, this increase in resistance can be measured in the form of a voltage pulse. The non-superconducting area is then cooled down by the cryogenic environment and returns to the superconducting state (iv—i).

One important technical detail is the fiber coupling of this detector because the efficiency and timing jitter depend on it. Depending on in which polarization the light hits the meander, the efficiency changes. When light hits the wire orthogonally polarized to the wire direction, the photon is less efficiently absorbed, than polarized parallel to the wire.

As seen in fig. 2.3 the coupled fibre in our characterized detector is parallel polarized to the nanowire. Moreover, to cover the whole light, shined out of the fibre, the geometry of the detection zone is constructed as a round plate and has roughly the same diameter as the fibre output (FC/PC). A smaller area would risk not absorbing each photon and a larger area would increase the time leading the signal to the computer unit.

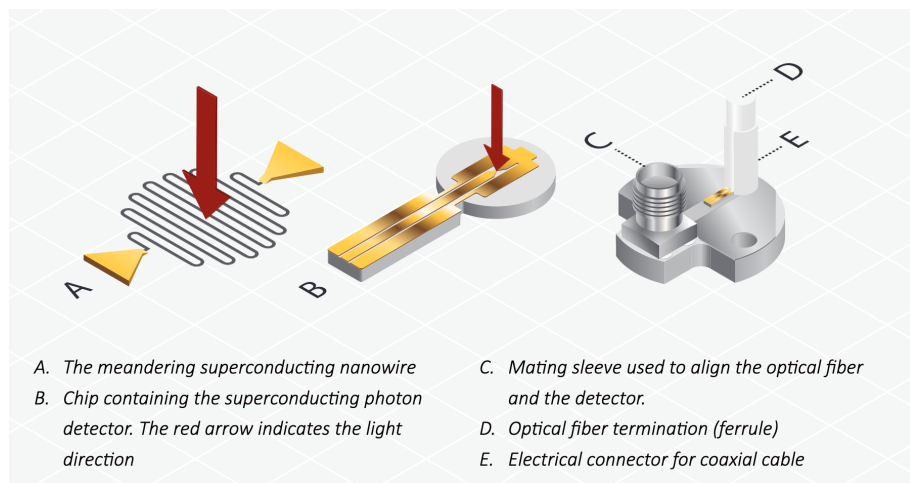


Figure 2.3: Scematic set up of the fiber coupling of a superconducting nanowire single photon detector [Zitieren!](#)

CHAPTER 3

Faint laser source for detector characterization

Counting photons one has to consider the characteristics of the emitter source as well. Here I focus only on the characteristics of a laser source affecting the characterization I made. For this first, I briefly sum up characteristics of a laser light source and its conditions it gives us for our detector characterization. Further, I make considerations regarding the inherent blindspots of laser light due to the randomness nature of photons in coherent light. Afterward, I introduce the setup I build for characterizing our SNSPD.

3.1 Characteristics of faint laser sources

Using a laser source enables us, considering the emitting light as monochromatic beam with angular frequency ω and constant Intensity I . The Photon flux of a laser is defined as the photon average number passing through a cross-section in unit time:

$$\Phi = \frac{IA}{\hbar\omega} = \frac{P}{\hbar\omega} \text{photons } s^{-1} \quad (3.1)$$

where I is the current of photon, A the cross-section, P the laser power and ω the angular frequency which depends on the wavelength.

The average number of registered counts $N(T)$ for a given detection time T by a detector is given by:

$$N(T) = T\Phi\eta = \frac{PT\eta}{\hbar\omega} \text{photons} \quad (3.2)$$

and hence the registered counts R per unit time by:

$$R = \frac{N(T)}{T} = \eta\Phi = \frac{P\eta}{\hbar\omega} \text{photons } s^{-1} \quad (3.3)$$

where η is the efficiency of the detector system.

This detection count rate is restricted by the largest amount on the dead time of the detector.

$$\mathcal{R}_{\max} \propto \frac{1}{\tau_d} \quad (3.4)$$

Because the used laser has a minimum threshold power which corresponds to a photonrate above the maximum one, one has to attenuate the laser power in order to detect all events.

The photon statistic of coherent light, in our case (in reasonable approximation) of our laser light, is given by poisson statistics. This characteristic stems from discrete nature of photons and hence non-equidistant spacing between photons. Measuring single photons, one has to ensure that we have a neglectable amount of photons in the segment of the deadtime because else our light characteristics inherently forbid us measuring each of the incoming photons.

This is calculated by looking at the propability of measuring one photon per length segment, given by the deadtime. First, we consider one Length segment given by the deadtime τ_d and the measurement time τ_m :

$$L_d = \frac{c}{\tau_d} \quad (3.5)$$

$$L_m = \frac{c}{\tau_m} \quad (3.6)$$

Through this, we can calculate for a given measurement time the average photon rate per length segment L_m and further the probability of finding one photon in the particular line segment L_d :

$$\bar{n} = \Phi \frac{L_m}{c} \quad (3.7)$$

$$p = \frac{\bar{n}}{N} \quad (3.8)$$

Where $N = \frac{c}{L_d}$ are the subsegments of the measured length segment L_m .

This enables us to calculate the probability p of finding n Photons per deadtime segment L_d and including this in our measurements.

3.2 Experimental setup

Though not measured by ourselves first, it is known from [Zitat](#) deadtime of the detector is around 20-25ns. This gives us a theoretical maximum detection rate of $\mathcal{R}_{\max} \propto \frac{1}{\tau_d} = 25 - 50\text{MHz}$. In order to realize the laser attenuation the following setup was build:

The first coupling of the laser light was done in order to operate with the beam on a lower stage, because the laserbeam was due to its construction on an uplifted stage. Afterward the beam passes a pbs to filter the horizontal polarized E field out. Further a galilei telescope was build out of one focal and one diffusing lens for minimizing the beam width so it fits fully on the surface of the AOM crystal. The first order of the AOM was set for flexible voltage modulation of the laser. A cover

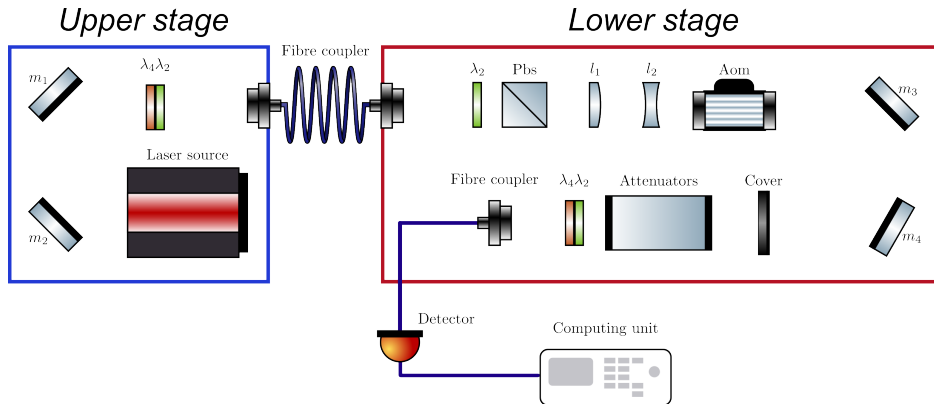


Figure 3.1: Setup for the SNSPD characterization (Need to be updated)

was used to filter out the first from the zeroth order of the AOM. Then a flip mount was placed, where Neutral density (ND) filters could be placed in and flexible placed in and out of the laser beam. The ND filters have the function to attenuate the laser light. At the end, before the laser light was again coupled in two waveplates where used to stabilize the light polarization regarding the slow axis of the fibre. Afterwards the light was coupled back into a fibre, so it can be send to the detector. It was important that the light was coupled in to a APC/PC to FC/PC optical fibre because the detector only had a FC/PC optical fibre input, in order to maintain higher efficiency coupling in the light.

Besides, this optical setup had to be protected from environmental light. For this, the room where the setup was running was shielded with alu foil which has a reflection coefficient of almost 90% at the operating wavelength of 780nm. Moreover a black box was build. It has the function to avoid further environmental light coupling into the fibre. Additionally, the optical fibre running from the optical setup to the detector was shielded with alu foil as well to avoid absorption from the optical fibre.

Neutral density (ND) filter calibration

We exactly need to know how many photons (related to Power) hit our detector. For this we need to measure the power (or number of photons) of the laser light we shining on the detector. The light we want to shine on the detector is very weak. So weak, we cannot measure it with powermeters or any other measurement devices (except with the uncharacterized detector). This weak power cannot be reached by regulating the laser power down by the laser device (why not? laser minimum power function only with a power higher than required), but has to be done by Neutral Density filters. So our laser power we send to the detector depends on ND filter.

Now there are two challenges relying on ND filters. First, since the fabric values are not precise, the filters need to be calibrated ourselves. Second, one single ND filter cannot attenuate the laser power enough and therefore one has to stack several density filters on each other, since their OD values are adding up.

From these two constraints, we need to calibrate the ND filters carefully, to get precise and accurate OD values of the ND filters.

To get accurate results, we measure the OD value with two methods to rule out systematic errors in our results. The first method measures the OD values, where the ND filters are set in the flip mount as described in graph ???. The second method measures the OD values after the fibre coupling directly in front of the powermeter outside the blackbox.

The attenuation of ND filters is quantized by the Optical density (OD) value. The measurement of the OD values done by sending light on the filter and measuring the power with and without the filter. The OD value is then calculated by the logarithmic value of the inverse transmission value. The transmission value is given by the proportion of the power with the filter compared without the filter.

Afterward, the final OD values of each method were averaged and the corresponding systematic and statistical errors are considered to get the closest to the true OD value for the ND filters.

Based one these OD values each measurement involving the laser was done.

- Basics of photon distribution of laser, attenuation, poisson statistics
- Set up for laser attenuation
- Single Photon Detection paper

CHAPTER 4

Characterization of a SNSPD by Single Quantum

In literature, four central characteristics have emerged to quantify the quality of single photon detectors and make their performance comparable. These characteristics are the system detection efficiency η_{sde} , the dark count rate (DCR), the recovery time ($\tau_{recovery} = \tau_{rec}$) and the timing jitter. In this thesis, I focus on the detector efficiency η_{sde} , the dark count rate (DCR) and the recovery time (τ_{rec}). With its importance will be dealt in the single sections. In general there are more than these introduced figures of merits, like after-pulsing but will not be considered in this thesis.

4.1 Dark Count Rate

The dark count rate (DCR) is the rate of measured detection events not intentionally sent from the source (here the faint laser source). It is measured in counts per second and can be caused by statistical fluctuations in the measurement electronics or by scattered or ambient light from the environment. A low DCR is important and allows differentiation between intended detected counts from the source and detected counts by environment and electronic noise. Furthermore, an increase in the count resolution is achieved by low DCR, enabling the detection of high signal-to-noise ratios at lower input frequencies.

In the context of SNSPDs, the DCR is dependent on the bias current applied to the nanowire. This is due to the fact that if the bias current approaches the critical current, the electronic fluctuates more frequently and exceeds more frequent the critical current which results in a triggered pulse. Furthermore, it is important to perform DCR measurements first in the characterization process because it determines the limit, where general measurements are not distorted by high DCR noise. Consequently, modifications to the DCR configuration serve as the baseline for all subsequent measurements with the detector and the associated setup.

Measurement and results

In order to evaluate the DCR, it is necessary to perform measurements in two different setups. First, a setup in which the detector is disconnected from the source and covered entirely in darkness. In such a setup, it can be assumed that no photons from the surrounding environment are striking the detector. This allows for the measurement of the DCR only triggered by the electronics noise depending on the detector's operating mode.

Depending on the operation mode means, the probability a signal is triggered by the detector raises if the bias current increases, hence the difference $\Delta I = I_c - I_B$ to the critical current decreases. This is due to the lower current gap its needed exceeding the critical current.

The measurement setup for this consists out of the detector with the protection cap on the output port of the detector. This configuration represents as described the most shielded environment from external light sources and serves as the reference value for optimal DCR values. The measurement was conducted by sweeping the bias current from 0 to 35 μA in 0.1 μA increments with an integration time of the count rates for 200 ms. The result is displayed in fig (b).

The second setup involves connecting the detector to the faint laser source of section 3.1. This is done in order to check how isolated the experimental set up. Moreover, one can use the comparison to the first set up to adjust the setup in order to minimize noise from the environment. This allows the optimal experimental configuration for the highest signal-to-noise ratio. For this it is assumed that the first setup has the lowest DCR. Again the bias current was swept from 0 to 35 μA in 0.1 μA increments with an integration time of the count rates for 200 ms. In fig (b) the results are shown for optimized and non optimized case.

At the initial, non optimized configuration an optical fibre was linked to the detector's output channel and the experiment's output connector. The laser source was turned off, so no signal noise except the described noises above trigger detection events. Afterwards, the optimized realization, the same connection was maintained, but the setup was fully protected by a self-constructed black box as showed in fig ???. Furthermore, the optical fibre was enclosed within an aluminium foil layer to prevent photons from coupling through the fibre's cladding.

As expected, the DCR raises in each case in (b) and (a) with decreasing difference $\Delta I = I_c - I_B$ due to raising probability that weak electronic noises trigger a signal. The orange course in (b) demonstrates that in the absence of protection, a significant number of photons from the environment are able to enter to the detector through various potential pathways like the fibre cladding and the coupling connection to the experiment.

In contrast, the fully protected setup, shown by the green course, exhibits an analogous course to the setup with the cap on fig 4.1(a). The results show, that the DCR of the coupled and protected setup is comparable to the DCR with a cap on. The peaks in the green course at ≈ 3 and $\approx 14\mu\text{A}$ are artifacts resulting from some leakages in the protection. Nevertheless, these leakages are not substantial when viewed in the context of the total photon count, particularly when considering the anticipated photon rates from the faint weak laser source operating in the high kHz and MHz frequency ranges.

Lastly, one can conclude from the investigation of the DCR of channel 1, that all further measurements have to be done at a bias current of $I_B < \approx 32\mu\text{A}$. To get a final figure of merit for the DCR of channel 1 , all counts up to the high raise are averaged and a measurement error of 1 Hz was estimated. The final DCR of this channel yields $(0.5 \pm 1)\text{Hz}$. Thus, measurements up to the predetermined limit are accompanied by a DCR of $(0.5 \pm 1)\text{Hz}$.

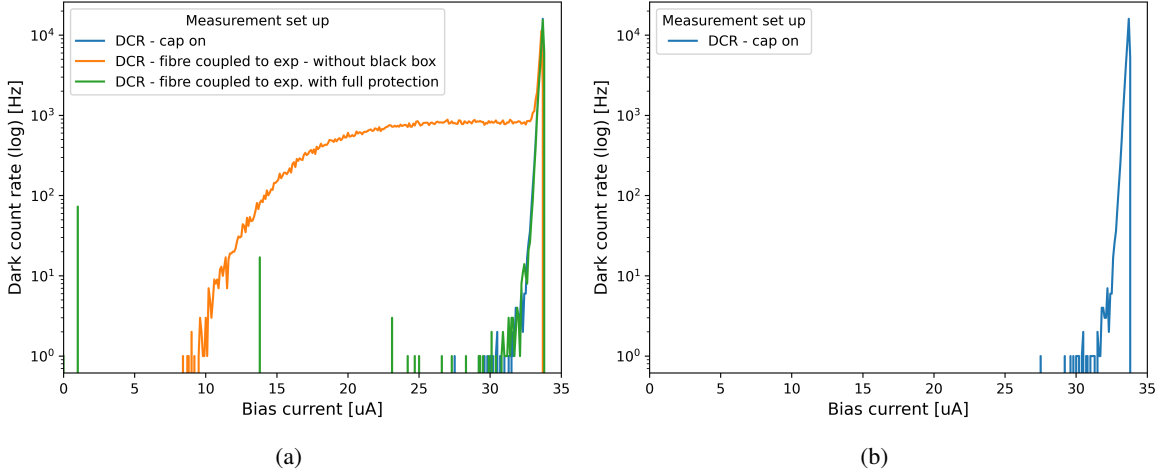


Figure 4.1: (a) Dark count rate (DCR) where the output channel of the detector which was protected by an aluminium cap. (b) Dark count rate (DCR) of both measurement realizations, compared to the DCR with the cap on.

4.2 Recovery time

The concept of the recovery time is visually depicted in fig 4.2. When a photon hits the detector and is absorbed, the efficiency of the detector drops to zero and no further photons can be measured for a certain period of time. This elapsed time is called the dead time τ_d . The efficiency then rises again to its original device efficiency η_G . This period is called the reset time τ_r . The characteristic curve between these two times forms the start of the increase to full efficiency. Moreover, the course to the original device efficiency η_G is not as depicted in fig 4.2 and serve only for visualization purposes. Finally, the sum $\tau_{rec} = \tau_r + \tau_d$ of both times forms the recovery time τ_{rec} .

The recovery time is important because it determines the rate the detector can detect photons. As lower the recovery time, as higher the counting rate.

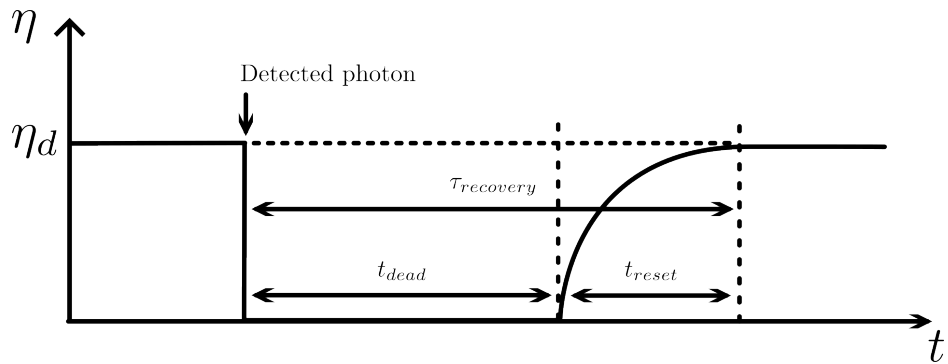


Figure 4.2: Schematic efficiency curve for the detection of a photon[3]. On the Y axis is the efficiency η , where η_G is the device efficiency. On the X axis is the time course of the efficiency

Measurement and results

In this work the recovery time measurement of this detector is based on an autocorrelation method of a continuous wave laser source (faint laser source) and was performed already by other groups [4, 5]. The measurement was conducted with the setup shown in fig 4.3. The raw analog signals from the detector were directly transmitted to a time tagger unit (Time Tagger 20) by Swabian instruments ([link](#)) with self-adjustable trigger voltages, a device deadtime of 6ns and a maximal counting rate of 9MHz.

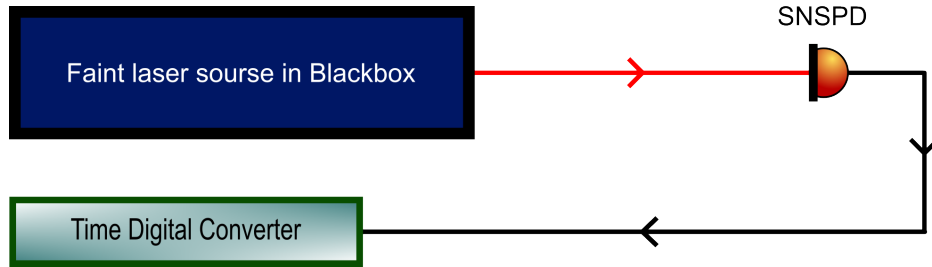


Figure 4.3: Experimental setup for measuring the recovery time. Optical setup of "faint laser source in black box" is depicted in 3.1

This unit enabled the tagging of incoming signals with a time tag, as implied by its name. Subsequently, the tags were used to process the time distances between all signals. The histogram of these distances provide an autocorrelation in time (here not normalized). The autocorrelation was measured for one channel for four different bias currents (26, 28, 31 and 31.2uA) and trigger voltages (300, 400, 500 and 600mV).

These measurements were done to determine the recovery time and analyze it dependencies. Results of the autocorrelation from two out of four bias current dependencies are presented in fig 4.4. The remaining other two bias current dependencies are shown in the appendix A.

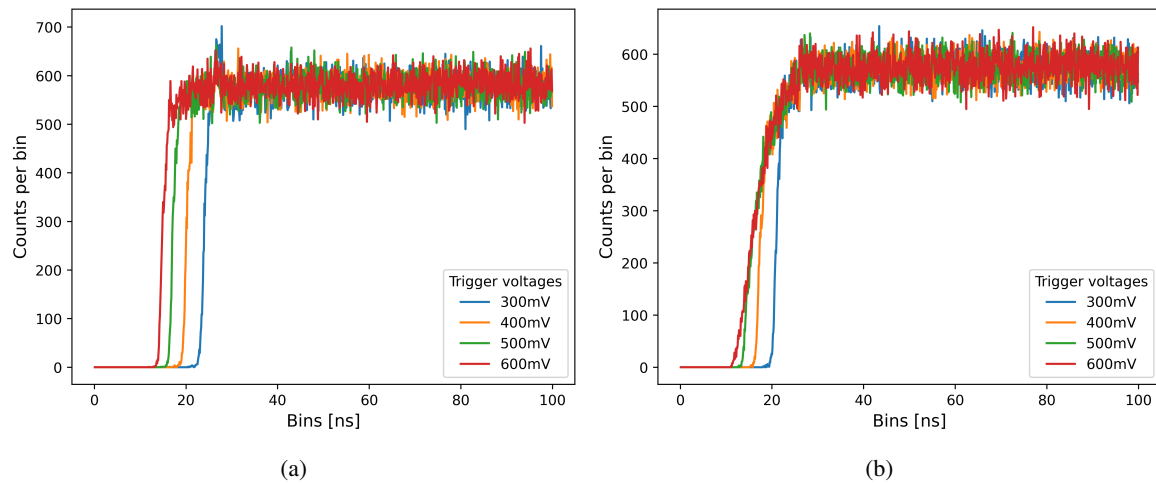


Figure 4.4: (a) Autocorrelation of distances between signals for $I_B = 31.2\mu A$ and (b) $I_B = 26\mu A$

The results of the autocorrelation show three major trends. First, for low trigger voltages, the dead

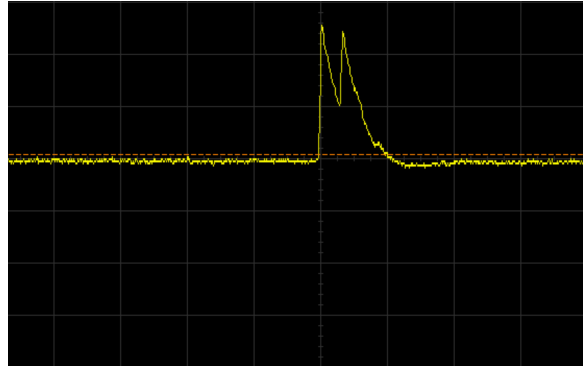


Figure 4.5: Analog signal screenshot of an oscilloscope from channel 1 for a bias current of 31.2uA and a trigger of 600mV. X-axis: time in 50ns steps (straight vertical yellow lines), Y-axis voltage in 500mV steps (straight horizontal yellow lines)

time is longer and decrease for increasing trigger voltages. This can be seen for the lower and higher bias current. The reason for this behavior can be explained best by looking at an exemplary raw analog signal (see fig 4.5) of two consequent pulses. One can see two pulses, where the second signal comes close ($\approx 20\text{ns}$) after the first one. So it is a pulse on the falling edge of the first one. Physically, that means, while the current in the superconducting wire wasn't fully at the default bias current of 31.2uA, a second photon, during τ_r , already hit the detector and got absorbed. If the trigger is below 500mV the time tagger will count this signal as one count, since the second pulse came when the remaining voltage of the wire was above 500mV. However, if the trigger is over 500mV both consecutive pulses will be counted by the time tagging unit as single counts. This allows more individual pulses to be counted separately with small gaps as close as the deadtime between them. However, only with a lower efficiency as depicted in 4.7, since in the time regime τ_r , the nanowire has not fully recovered yet. Therefore, we see this earlier raise in fig 4.4.

Secondly, for the lower bias current (26uA), the slope tends to decrease towards the end of the saturation point. Moreover, the courses of the raising counts for each trigger voltage are converging towards each other earlier. In comparison, with a bias current of 31.2uA the four different courses are separate till they reach their peak. This can be explained by the fact that, depending on the bias current, the triggered resistance caused by a photon hitting the superconducting nanowire is different. This behaviour can also be verified by the different pulse heights of the signals in fig: ???. According to Ohm's law, a low bias current corresponds to lower voltage pulses and vice versa, for the same resistivity. This is also comprehensible by Ohm's law. Due to the lower pulse, the regime, where one pulse can be resolved by a trigger voltage of 600mV but not 500mV becomes smaller. Hence, one can see that the counts per bin equalize for increasing time distances.

The third trend concerns the small peak, in the range of 24-27ns as can be seen clearly in the course with a bias current of 31.2uA 4.4(a). This small peak is more suppressed with a lower bias current and higher trigger voltages. Closer examination of this trend are shown in the appendix A. A plausible solution for this behaviour can be understood with the fig 4.6.

Following the detection of a current, the course of the current does not proceed directly and precisely to the bias current. Instead, it oscillates for a brief period and then rapidly reaches equilibrium. In the small oscillating period, the Dark count rate raises exponentially (seen in fig: 4.1(b)) and adds to the detected counts. It can be concluded that the optimal recovery time is achieved when the detector is

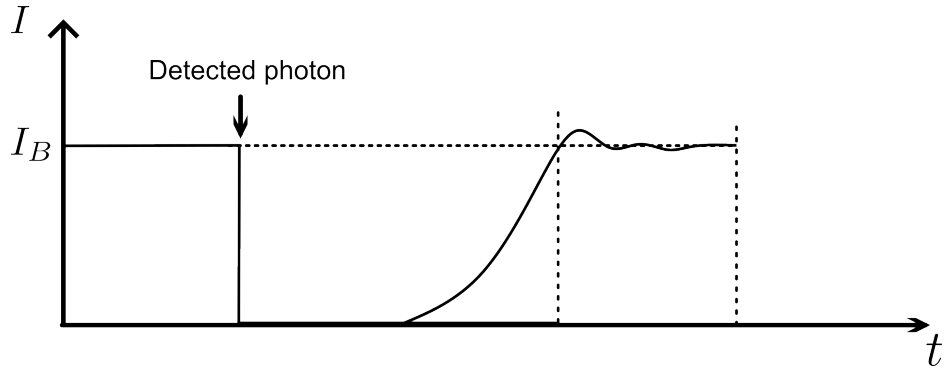


Figure 4.6: Sketch of brief oscillating current and subsequent levelling to the bias current

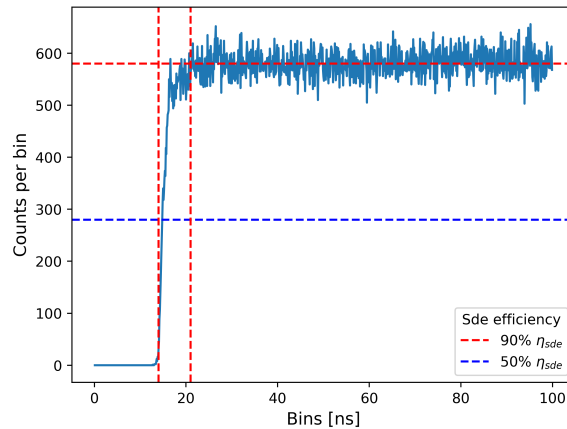


Figure 4.7: Histogram of distances between signals for $I_B = 31.2\mu A$ and 600mV. H- and v-lines indicate the dead-; reset- and recovery time

operated in closeness to the bias current. This enables the generation of a higher pulse, which in turn results in a steeper reset time, a smaller dead time, and consequently, a shorter recovery time.

DISCLAIMER: ALL THE RESULTS AND METHODS ARE NOT FINALIZED AND WILL BE ADAPTED, IF METHOD IS AGREED

Finally, a reasonable trigger point for a bias current of $31.2\mu A$ is 600mV, which yields to the lowest recovery time. The calculation of the τ_{rec} is done, by calculating the average of counts per bin from $30\mu A$ till the end. Here, I chose $30\mu A$ as the starting point, because from this point a clear saturation and a constant course is visible. Furthermore, I fitted a function to estimate the point were 50% and 90% of the full efficiency is reached. Moreover, the raise of the function for the dividing line between dead and reset time is calculated by the point where the gradient of the fitting function is not zero any more. The calculated points are visualized in fig: 4.7 and the final recovery time is $\tau_{rec}^{90\%} = (21.21 \pm 0.34)\text{ns}$, where $\tau_d = (14.13 \pm 0.14)\text{ns}$ is the dead time and $\tau_r = (7.08 \pm 0.36)\text{ns}$ the reset time. Moreover, the time the detector is back at efficiency of $\eta_{sde} = 50\%$ is $\tau_{rec}^{50\%} = (18.21 \pm 0.24)\text{ns}$.

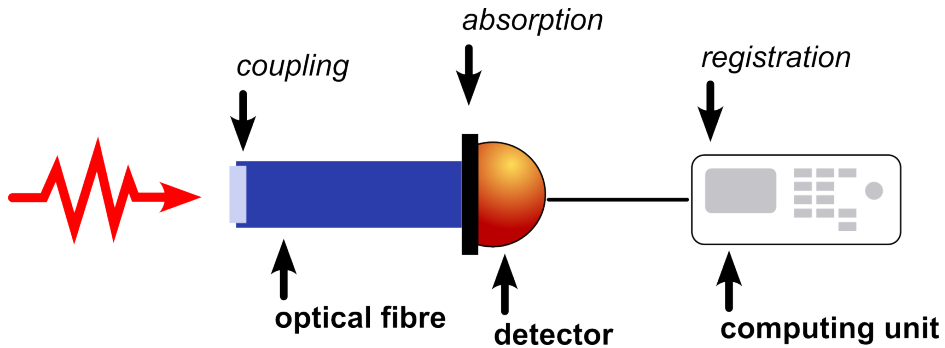


Figure 4.8: Sketch of the components in the detector setup where photonlosses appear and consequently a probability (η_K , η_A or η_R) has to be considered.

4.3 Efficiency

There are three types of efficiencies that describe independent loss processes in single photon detection. An efficiency can be equated with the probability that a quantum mechanically process under consideration will occur.

These three efficiencies are the coupling efficiency (η_K), the absorption efficiency (η_A) and the registration efficiency (η_R). The graph 4.8 shows schematically where the different loss in the detection process appears. When a photon is sent to a detector via an optical fibre, not all photons can be coupled into the fibre. The probability of coupling is called the *coupling efficiency*. When photons hit the detector, there is always a probability that the photon will not be absorbed by the detector. This is due to material and symmetry properties. This is described by the *absorption efficiency*. Finally, there is always a probability that the photon will not be registered by the measuring electronics. This is expressed with the *Registration efficiency*.

In literature, these terms are summarized in two general efficiency terms: the device detection efficiency ($\eta_{dde} = \eta_A \cdot \eta_R$) and the system efficiency ($\eta_{sde} = \eta_A \cdot \eta_R \cdot \eta_K$) [6]. The device's efficiency η_{dde} corresponds to the efficiency of the device itself, when photons are sent to the detector in a free environment without any fibre coupling. In this way only the efficiency of the elements detecting photons are considered. The system detection efficiency η_{sde} takes the coupling losses to the optical fibre into account. This is the case if the detector is connected to a fibre, as the device properties or the experiment does not allow photon detection in a free environment.

Measurement and results

DISCLAIMER: ALL THE RESULTS AND METHODS ARE NOT FINALIZED AND WILL BE ADAPTED, IF METHOD IS AGREED

In the given setup, only the system detection efficiency c is measured, because the detector is already prebuilt with a fixed coupling to a fibre. This internal fibre is connected to a fibre to fibre port (FC/PC to FC/PC). Through this one, one can connect the detector with an external fibre and send photons from the experiment to the detector.

The system detection efficiency η_{sde} is measured in different ways, each pointing out a different dependency. Each measurement was done in the setup explained in part 3. In addition, the order of

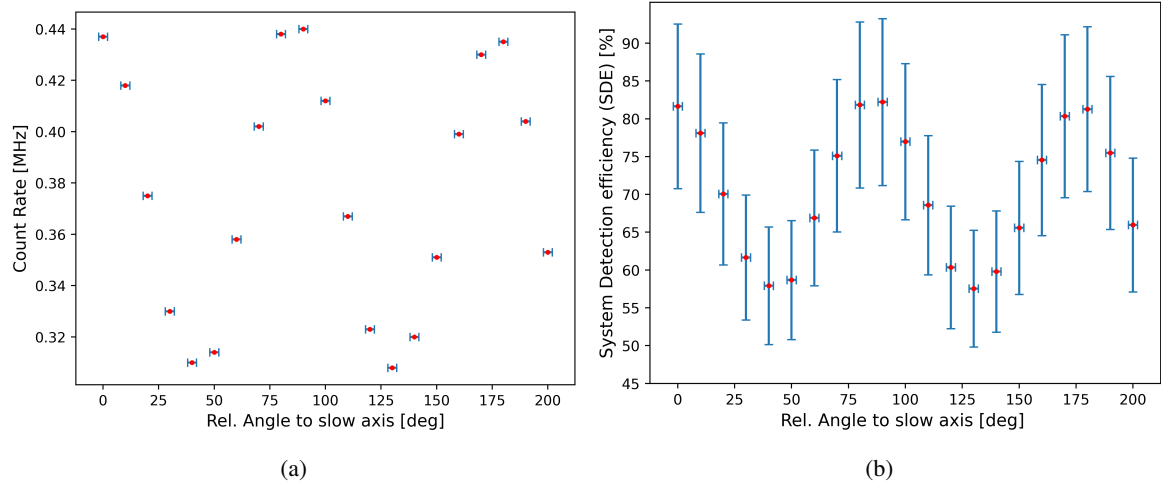


Figure 4.9: (a) Angle dependent countrate (b) Angle dependent system detection efficiency η_{sde}

the measurements is a relevant factor, as the conclusions drawn for one measurement influence the preceding measurements.

In conclusion, it is first necessary to align the polarization of the laser light with the slow axis of the fibre connected to the output port of the detector. Along the manual the coupled light needs to polarized along the slow axis of the fibre [**manual_single_quantum_snspd**]. This is explained by the technical fact that only the slow axis of the fibre is coupled to the output port of the detector. The reason for this preselection of polarization is the related maximum η_A , explained in part 2.

By adjusting the laser beam linear with a quarter-wave plate first and rotating the half-wave plate in 10 degree steps afterwards, the polarization axis was rotated. With this, it was possible to find the angle configuration were the maximum of light was coupled to the slow axis of the fibre. This is important since measuring subsequent efficiency measurements aligned to a different axis would put a systematic downshift on the true efficiency of the detector.

In the figures 4.9(b) the count rate and the resulting system detection efficiencies are depicted. For preceding measurements the polarization was aligned to an angle, where a maximum of $\eta_{sde} = 81.652 \pm 10.872$ was reached.

In a second measurement the bias current und trigger voltage dependency was investigated. For this the bias current was swept from 0 to 35uA in 0.1uA steps and events within 200ms integration time were counted.

In fig 4.10 one can see that at lower trigger voltage of 300mV the count rate oscillates a bit, which again corresponds likely to the increased dark count rates as explained in 4.6. Furthermore, one can see that for lower trigger voltages the detected counts for lower bias currents are higher. This is due to the consideration of lower voltage pulses in lower bias current regimes if the trigger voltage is low. Hence, with a lower trigger voltage one can count already signals, however, with a very low system detection efficiency η_{sde} . Another behaviour is the saturation, which is reached by each trigger voltage configuration at around $I_{Bias} \approx 20\mu A$. Here the maximum count rate is reached and the efficiency course continues constant without any gradient. At the end at a bias current of $I_{Bias} \approx 32\mu A$ the efficiency drops. This is because the critical current is reached. After this, along

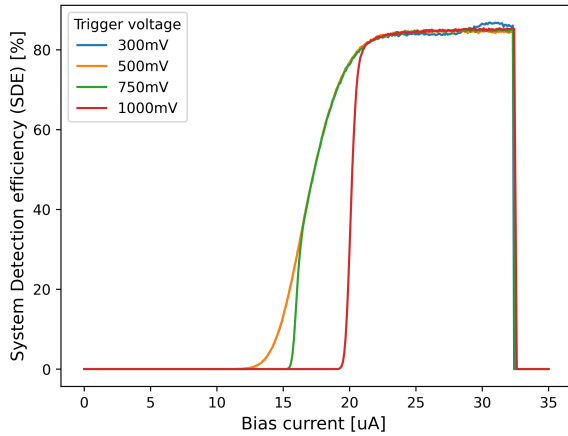


Figure 4.10: System detection efficiency for different bias currents and trigger voltages

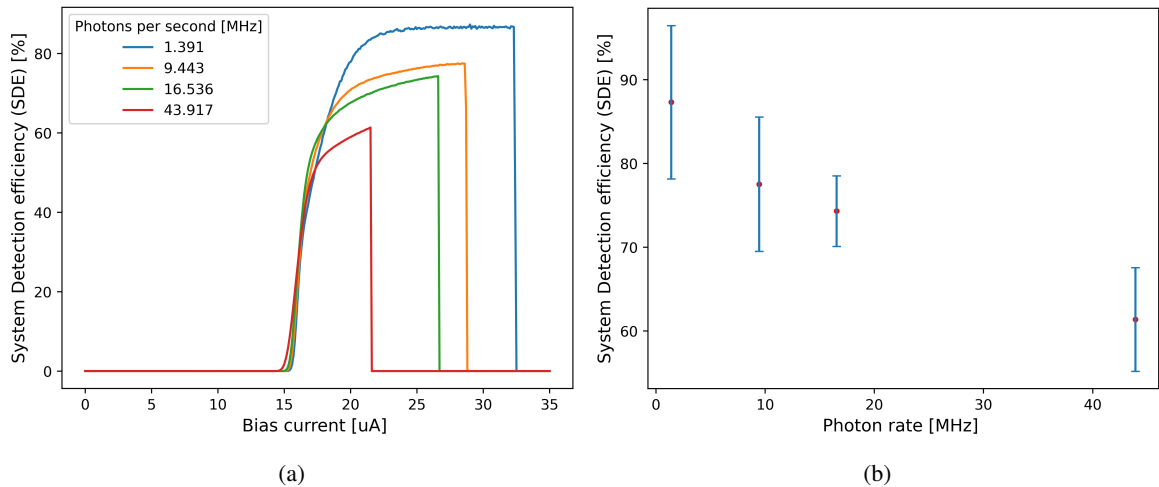


Figure 4.11: (a) Course of system detection efficiency for different bias current and count rates (b) Course of system detection efficiency for different count rates

the **[manual_single_quantum_snspd]**, the detector stops sending countable analog signals, which corresponds to an efficiency of zero.

Finally, measurements for different count rates were done, to determine the bandwidth where the photons are detected with the highest efficiency. The count rates were varied by using different ND filters and was done by putting together different ND filter combinations in order to get different OD values and therefore different count rates. To avoid the oscillation of count rates near the critical current as seen by the blue course in fig 4.10 a trigger voltage of 750mV is used.

In fig 4.11(a) one can see that the system detection efficiency is decreasing with increasing count rates. Moreover, only for the measurement of 1.391MHz one gets a range of bias currents where the efficiency is constant. All the other measurements with higher count rates show a continues increase in η_{sde} up to the point the detector shut down. Furthermore, the shut-down happens earlier, when the count rate is higher. This dynamics follows from the fact that the detector is not able to recover in

time, when the count rate is too high. Hence, the critical temperature is reached earlier, when the count rate is raising and the detections is shut down.

In fig 4.11(b) the maximum system detection efficiency for each count rate is shown. One see clearly a downward trend for raising count rates. Moreover, the measurement shows the saturating and therefore a maximal system detection efficiency of $(87.308 \pm 9.159)\%$ for channel 1. This η_{sde} is reached at a count rate of $1.391 \pm 0.32\text{MHz}$.

4.4 Discussion

CHAPTER 5

Conclusion and Outlook

APPENDIX A

Appendix

In the appendix you usually include extra information that should be documented in your thesis, but not interrupt the flow.

Bibliography

- [1] G. A. Steudle et al.,
Measuring the quantum nature of light with a single source and a single detector,
Physical review. A, Atomic, molecular, and optical physics/Physical review, A, Atomic,
molecular, and optical physics **86** (2012),
URL: <https://doi.org/10.1103/physreva.86.053814> (cit. on p. 2).
- [2] singlequantum.com, *Superconducting Nanowire Single Photon Detectors Operation principle*,
<https://singlequantum.com/wp-content/uploads/2023/06/Single-Quantum-Operation-Principle-print.pdf>, Accessed: 2023-06, n.d. (Cit. on p. 3).
- [3] K. Shalm et al., *Single-Photon Detector Tutorial*, Computer Scientist QCRYPT,
National Institute of Standards and Technology, 2013, URL:
<https://qcrypt.github.io/2013.qcrypt.net/contributions/Shalm-slides.pdf>
(cit. on p. 11).
- [4] C. Autebert et al.,
Direct measurement of the recovery time of superconducting nanowire single-photon detectors,
Journal of applied physics **128** (2020), URL: <https://doi.org/10.1063/5.0007976>
(cit. on p. 12).
- [5] S. Miki, M. Yabuno, T. Yamashita and H. Terai, *Stable, high-performance operation of a fiber-coupled superconducting nanowire avalanche photon detector*,
Optics express **25** (2017) 6796, URL: <https://doi.org/10.1364/oe.25.006796>
(cit. on p. 12).
- [6] C. M. Natarajan, M. G. Tanner and R. H. Hadfield,
Superconducting nanowire single-photon detectors: physics and applications,
Superconductor science and technology/Superconductor science technology **25** (2012) 063001,
URL: <https://doi.org/10.1088/0953-2048/25/6/063001> (cit. on p. 15).